

The role of annealing in determining the yielding behavior of glasses under cyclic shear deformation

Himangsu Bhaumik,¹ Giuseppe Foffi,² and Srikanth Sastry^{1,*}

¹Jawaharlal Nehru Center for Advanced Scientific Research, Jakkur Campus, Bengaluru 560064, India.

²Laboratoire de Physique des Solides, CNRS, Université Paris-Sud, Université Paris-Saclay, 91405 Orsay, France

Yielding behavior in amorphous solids has been investigated in computer simulations employing uniform and cyclic shear deformation. Recent results characterise yielding as a discontinuous transition, with the degree of annealing of glasses being a significant parameter. Under uniform shear, discontinuous changes in stresses at yielding occur in the high annealing regime, separated from the poor annealing regime in which yielding is gradual. In cyclic shear simulations, relatively poorly annealed glasses become progressively better annealed as the yielding point is approached, with a relatively modest but clear discontinuous change at yielding. To understand better the role of annealing on yielding characteristics, we perform athermal quasistatic cyclic shear simulations of glasses prepared with a wide range of annealing in two qualitatively different systems – a model of silica (a network glass), and an atomic binary mixture glass. Two strikingly different regimes of behavior emerge: Energies of poorly annealed samples evolve towards a unique threshold energy as the strain amplitude increases, before yielding takes place. Well annealed samples, in contrast, show no significant energy change with strain amplitude till they yield, accompanied by discontinuous energy changes that increase with the degree of annealing. Significantly, the threshold energy for both systems correspond to dynamical crossover temperatures associated with changes in the character of the energy landscape sampled by glass forming liquids. Uniform shear simulations support the recently discussed scenario of a random critical point separating ductile and brittle yielding, which our results now associate with dynamical crossover temperatures in the corresponding liquids.

The response of structural materials to applied stresses is of fundamental importance in determining their utility. Many structural materials are amorphous solids, with molecular glasses being a predominant example. In addition to specific types of molecular glasses, many other amorphous solids are the subject of ongoing fundamental and applied research investigations, such as colloidal suspensions, foams, emulsions and granular packings [1–4]. Upon increasing deformation or applied stresses, the mechanical response of such amorphous solids generically changes from elastic solid-like response at small deformations, to elasto-plastic flow at large deformations. But the transition between these two regimes occurs in diverse ways. For typical molecular glasses (window glass or silica, and metallic glasses), yielding is a sudden, sharp event, characterised as brittle failure. For many *soft* solids, the transition between the elastic and plastic flow regimes is gradual (ductile), with no sharply defined transition point between them. Prominent among the challenges in understanding yielding is the rationalisation of this diversity. A number of theoretical and computational investigations have recently addressed the nature of the yielding transition [5–22], many of which support the notion that yielding must be understood as a spinodal limit, at which system-spanning plastic deformation occurs discontinuously. The nature of such a limit (whether it is *critical* or not, and whether correlated plastic rearrangements or *avalanches* diverge upon approaching it, *etc.*) are matters of ongoing debate. Computational investigations have typically focused on the limit of ather-

mal quasistatic (AQS) deformation of atomistic models, employing both uniform [12–15, 20, 23, 24] or cyclic [8, 9, 16, 17, 19, 22] shear deformation, and simulations of elasto-plastic models [7, 20, 21]. Although the role of the degree of annealing in determining the mechanical response of glasses has been studied from early on [23, 24], the focus has been on features such as strain localisation, and not the nature of the yielding transition itself. Recently, Ozawa *et al.*, [20] investigated the dependence on annealing of the nature of yielding by considering uniform shear simulations of glasses prepared over a wide range of temperatures. Based on their numerical results and accompanying theoretical analysis, they identified two distinct regimes of annealing, one of high annealing in which yielding is discontinuous, and the other of poor where it is gradual, and argued that a random critical point (of the class described by the random field Ising model (RFIM)) separates the two regimes at a critical value of annealing (or disorder). Investigations employing cyclic shear deformation, with both poorly annealed and moderately well annealed glasses [17, 22] reveal an apparently different picture. For amplitudes of strain below a critical value, repeated cyclic shear results in annealing the glasses, with the degree of annealing increasing with an increase in the strain amplitude. Yielding (more precisely, *fatigue* failure) occurs discontinuously at a critical strain value, with a jump in the peak stress, the emergence of diffusive motion of particles, and shear banding [9, 16, 17, 19, 22].

An important question raised by the above results is whether uniform and cyclic shear protocols lead to qualitatively different manifestations of yielding behavior. Additionally, one may ask how general the results

* sastry@jncasr.ac.in

in earlier work [17, 20, 22] are, since the studied systems have all been models of atomic glasses. Finally, if a threshold degree of annealing or disorder does robustly separate brittle and ductile yielding behaviors, one may ask whether we can attribute any physical significance to the critical annealing. We address these questions in the present work. We consider cyclic shear simulations of a model atomic glass studied earlier (the Kob-Andersen binary mixture Lennard-Jones model (KA BMLJ)) [17, 22], but over a much broader degree of annealing. As an important example of a distinct class of glasses with which to study the generality of the aforementioned results, we study silica, a network forming glass. From the analysis of these two models, we conclude that cyclic shear indeed reveals the transition from ductile to brittle behavior, consistently with uniform shear investigations, revealing new and interesting characteristics of the transition. Finally, our results reveal an interesting physical significance to the critical degree of annealing – we find that the critical degree of disorder corresponds to well studied dynamical crossovers in the studied systems, the fragile-strong crossover in silica, and the mode coupling temperature in the KA BMLJ model.

For both the model systems we study, the glasses we subject to AQS deformation are generated by local energy minimization of simulated instantaneous liquid configurations. Based on the well studied relationship between temperature and energies of typical minima or *inherent structures* (IS) (*e. g.*, [25]; *Appendix*, Fig. A1), the degree of annealing of the glasses is equivalently specified by the potential energy of the inherent structures, or the temperature of the equilibrium liquid from which they are obtained.

We simulate the BKS model [26] of silica as implemented in Voivod *et al.* [27] for a temperature range from $T = 2500K$ to $6000K$, at density $\rho = 2.8\text{gm/cm}^3$ using $N = 1728$ ions. Arising from its tetrahedral local geometry, silica exhibits a liquid-liquid phase transition [28, 29], and an associated fragile to strong crossover [27, 30–32], which occurs around $T = 3100K$ for $\rho = 2.8\text{gm/cm}^3$, within the range of temperatures we simulate.

The KA BMLJ is simulated at reduced density $\rho = 1.2$, for $N = 4000$, for a temperature range from $T = 0.435$ to $T = 1.5$, corresponding to IS energies from $E_{IS} = -6.89$ to around -7.0 . We also study inherent structures obtained through a finite temperature, finite shear rate cyclic shear annealing procedure reported in [33], which extends the range of energies down to $E_{IS} = -7.07$ (to be compared to the extrapolated Kauzmann energy of $E_{IS}^K = -7.15$ [33]). We employ the same procedure for system sizes $N = 2000, 8000, 16000, 32000, 64000$, to obtain glasses with lowest energy $E_{IS} = -7.05$, for performing a system size analysis.

These initial inherent structures are subjected to athermal quasi-static shearing (AQS) protocol involving: (i) Affine transformation by small strain increments of $d\gamma = 2 \times 10^{-4}$ in the xz -plane ($x' \rightarrow x + d\gamma z$, $y' \rightarrow y$, $z' \rightarrow z$). (ii) Energy minimization. The strain γ is varied cycli-

cally: $0 \rightarrow \gamma_{\max} \rightarrow -\gamma_{\max} \rightarrow 0$ (or uniformly, for part of the study). Repeated deformation cycles for a given γ_{\max} result in the glasses reaching steady states wherein the properties on average do not change. Further details regarding simulations may be found in *Appendix* Sec. 1 and 2).

Cyclic Shear Deformation of BKS Silica

We first describe results from cyclic shear deformation of silica, which are shown in Fig. 1. In Fig. 1(a), we show for a wide range of temperatures the steady state (zero strain) energy U obtained in the limit of large numbers of cycles. The data shown are obtained by stretched exponential fits of the stroboscopic (at the end of each cycle, strain $\gamma = 0$) values of the energy as a function of the accumulated strain $\gamma_{acc} = 4 \times \gamma_{max} \times N_{cyc}$ where N_{cyc} is the number of elapsed cycles (Additional analysis data pertaining to Fig. 1 is found in Figs A2-A4 of *Appendix*). The data for the highest three temperatures, $T = 6000K, 4000K, 3500K$, reveal the yielding strain $\gamma_y = 0.23$ as a point of minimum energy, consistently with previous work [17, 22], but with a feature that was not clear in earlier work – as the yield strain amplitude $\gamma_{max} = \gamma_y$ is approached, the energy of all the glasses corresponding to this temperature range converge to a common energy value of -1867kJ/mol , corresponding to a temperature of $T_{th} = 3100K$. At lower temperatures, a surprising new feature appears – to a very good extent, the energies of the glasses do not change with γ_{max} , and at the yielding point (with a yield strain that increases mildly as the glass energy decreases), the energy shows a discontinuous jump, whose size increases as one goes to lower temperatures, as shown in the inset of Fig. 1(a). Both the relative lack of annealing during cyclic shear, and the increasing size of the energy jump upon yielding, are new features. Next we consider the variation of maximum stress σ_{xz}^{max} with strain amplitude for the different cases, and find (as shown in Fig. 1(b)) that the size of the stress jump at yielding increases with decreasing temperature/degree of annealing. At the highest two temperatures, our results indicate that the stress drop at yielding are very small, but increase rapidly below $T = 3100K$. In Fig. 1(c) we show energies through the cycle for the studied temperatures in the steady state, at the largest strain amplitude below yield, identified as the yield strain amplitude γ_y . These data reveal that (unlike the KA BMLJ; see below) observable plasticity remains even in well annealed samples in the steady state, a feature that merits further analysis. We extract the energy at zero strain, and at $\gamma = \gamma_y$ from this data, shown in Fig. 1(d), which clearly indicate that both the zero strain energy, and the energy at the yield strain, decrease below $T = 3100K$, but they do so differently. The difference between the two, which may be thought of as an energy barrier to yielding, increases with decrease of temperature below $T = 3100K$ (shown in Fig. 1(d) inset).

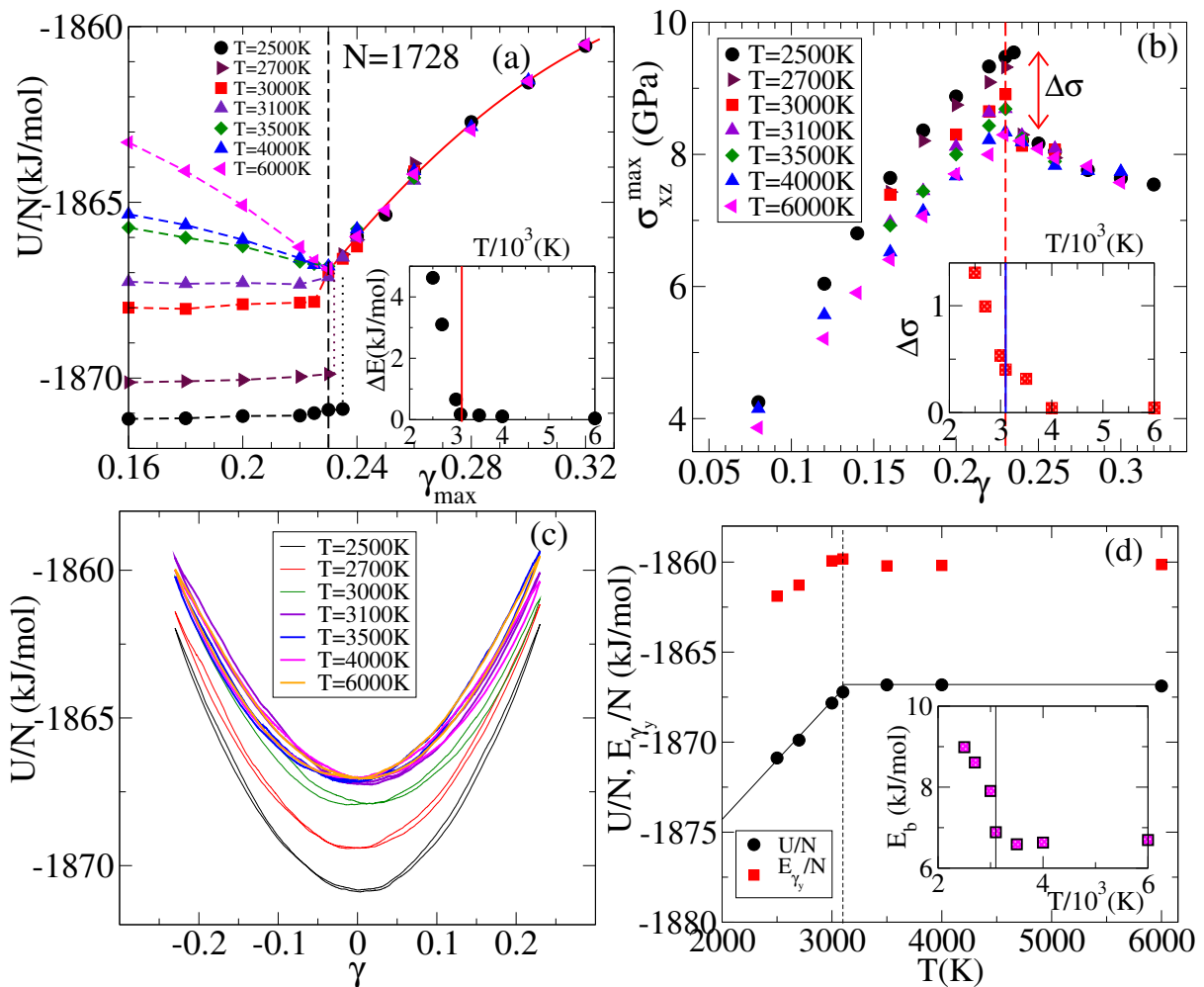


FIG. 1. **BKS Silica under cyclic shear:** ($N = 1728$) (a) The steady state energies (stroboscopic) are plotted against γ_{max} for different temperatures. Inset shows the jump in energy ΔE at the yielding point. (b) The maximum stress value is plotted against strain amplitude for different temperatures. The magnitude of jump in the maximum stress $\Delta\sigma$ at the critical strain is plotted against T in the inset. (c) Plot of the potential energy versus γ in the steady state for different temperatures, at the yield strain amplitude. (d) Plot of energies E_{γ_y}/N at $\gamma = \gamma_{max} = \gamma_y$, and U/N (at $\gamma = 0$) for the yield amplitude $\gamma_{max} = \gamma_y$ as a function of temperature. Inset shows the difference between E_{γ_y}/N and U/N vs. T . Vertical lines in the insets are at $T = 3100K$.

Cyclic shear deformation of the Kob-Andersen Binary Mixture Lennard-Jones Model

Given that the cyclic shear results for silica appear qualitatively different from the earlier results [17, 22] for the KA BMLJ, the natural question to address is whether the earlier observations change when one considers a broader range of IS energies for the initial glasses. We address this by considering initial energies from -6.89 to -7.07 , for $N = 4000$. The results shown in Fig. 2 reveal that indeed, by considering a larger range of annealing, the picture changes radically from that observed earlier. As seen in Fig. 2 (a) the energies vs. strain amplitude for different initial IS energies show a striking resemblance to the behavior seen in BKS silica. For initial IS energies above $E_{IS} = -6.99$, as the yield strain amplitude

$\gamma_{max} = \gamma_y$ is approached, the energy of all the glasses converge to a common energy value of -6.995 , corresponding closely to a temperature of $T_{th} = 0.435$. For lower initial IS energies, there is a near lack of annealing with strain amplitude below yielding, and a discontinuous change in energies is observed at yielding. More striking in this case compared to silica, however, is the significant increase in the yield strain values with greater annealing, reaching a maximum value of about $\gamma_y = 0.11$, compared to around $\gamma_y = 0.075$ for the poorest annealed glasses. The difference in the two cases is related to the more modest range of annealing achieved in the case of silica (Additional analysis data pertaining to Fig. 2 is found in Figs A5-A7 of *Appendix*). Fig. 2 (b) shows that the jump in the maximum stress grows strongly with annealing, and the inset of Fig. 2 (b) shows that the energy

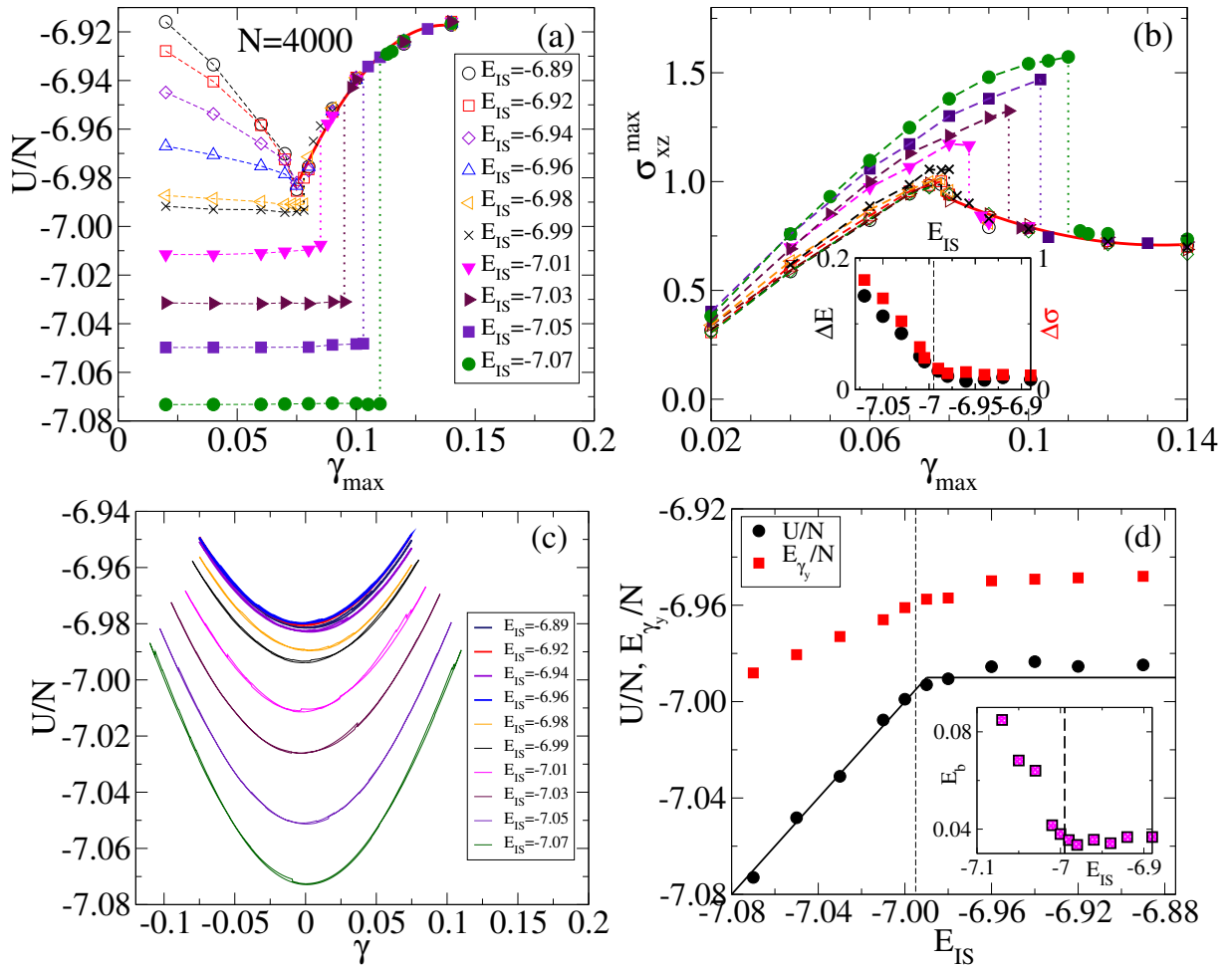


FIG. 2. **Kob-Andersen BMLJ under cyclic shear:** ($N = 4000$) (a) The steady state energies (stroboscopic) are plotted against γ_{max} for different E_{IS} . (b) The maximum stress value is plotted against strain amplitude for different temperatures. Inset shows the jump in the energy, ΔE , and the jump in maximum strain $\Delta\sigma$ at the yield strain, as a function of E_{IS} . (c) Plot of potential energy versus γ in the steady state, for different E_{IS} , at the critical strain amplitude. (d) Plot of energies E_{γ_y}/N at $\gamma = \gamma_{max} = \gamma_y$, and U/N (at $\gamma = 0$) for the yield amplitude $\gamma_{max} = \gamma_y$ as a function of E_{IS} . Inset shows the difference between E_{γ_y}/N and U/N vs. E_{IS} . Vertical lines in the insets are at $E_{IS} = -6.995$.

and stress jumps increase below $E_{IS} = -6.99$. In Fig. 2 (c) we show the steady state energies through the cycle just below the respective yield strains γ_y . Fig. 2 (d) shows the energies at the minimum, and at γ_y , and (in the inset) their difference, revealing a striking change of behavior below the threshold energy of -6.995 .

Taken together, the results for silica and the KA BMLJ strongly support a scenario that the nature of yielding changes drastically below a threshold degree of annealing. The main difference in comparing with uniform shear is that under cyclic shear, poorly annealed glasses evolve towards glasses at the threshold degree of annealing, and manifest a correspondingly mild discontinuous behavior.

Uniform shear of the Kob-Andersen Binary Mixture Lennard-Jones Model

Although results from cyclic shear simulations above provide results that are consistent with the ductile to brittle transition scenario discussed by Ozawa *et al.* [20], neither model has been studied in sufficient detail with uniform shear to allow a direct comparison. In order to make such a comparison, we study the response to uniform shear of the KA BMLJ model, for a wide range of annealing of the glasses and system sizes, and obtain results consistent with [20]. In Fig. 3 (a) we show the sample averaged stress-strain curves for $N = 64000$ over the studied range of glass energies. We see that as E_{IS} decreases, the yielding transition becomes progressively sharp. Likewise, the transition becomes sharper with system size, as shown in Fig. 3 (b) for $E_{IS} = -7.05$, supporting a discontinuous, first order transition in the ther-

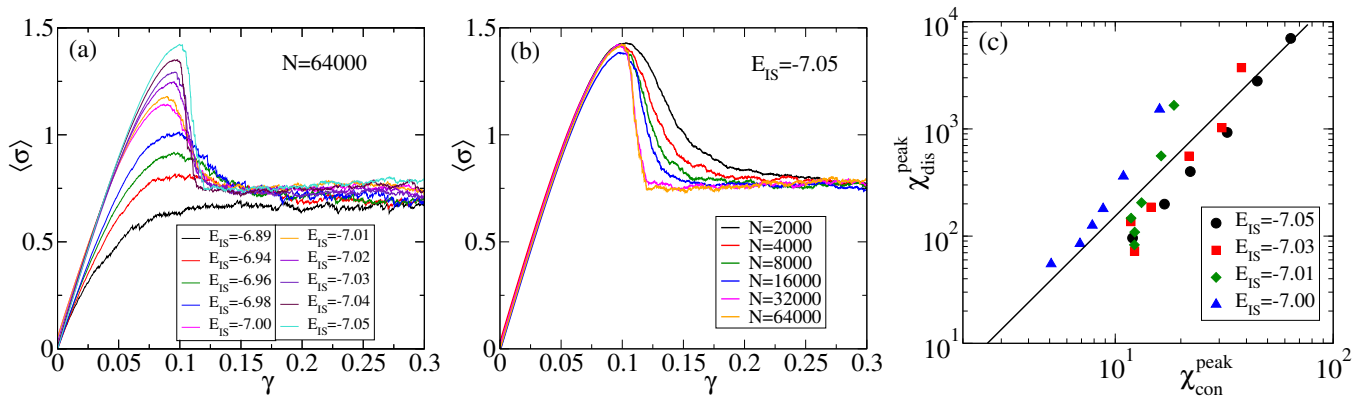


FIG. 3. **Kob-Andersen BMLJ under uniform shear:** (a) Stress-strain curves for different E_{IS} for $N=64000$ averaged over several samples. (b) Stress-strain curves for $E_{IS} = -7.05$ for a range of system sizes. (c) Scatter plot of the $\chi_{dis,peak}$ against $\chi_{con,peak}$ for different E_{IS} below annealing threshold to show agreement with $\chi_{dis,peak} \sim \chi_{con,peak}^2$.

modynamic limit. We compute two associated susceptibilities, the "connected" susceptibility $\chi_{con} = -\frac{d\langle\sigma\rangle}{d\gamma}$ and the "disconnected" susceptibility $\chi_{dis} = N[\langle\sigma^2\rangle - \langle\sigma\rangle^2]$, where the averages are over samples (shown in *Appendix*, Fig. A8, along with related results). Both quantities grow with system size (with peak values $\chi_{dis}^{peak} \sim N$, and $\chi_{con}^{peak} \sim \sqrt{N}$), and as shown in Fig. 3 (c) are consistent with $\chi_{dis}^{peak} \sim \chi_{con}^{peak^2}$, as would be expected when disorder-induced sample to sample fluctuations dominate in determining the susceptibilities [20].

Dynamical Crossover

The threshold annealing level for BKS silica and the KA BMLJ correspond respectively to $T = 3100K$, and $T = 0.435$. To investigate the meaning of these crossover temperatures we consider the dynamics of the respective liquids. In Fig. 4, we show the α relaxation times of the two systems *vs.* temperature. The self part of the intermediate scattering functions from which the relaxation times are obtained are shown in Fig. A9 in *Appendix*. For silica, we see that the relaxation times τ_α show a fragile to strong crossover, as reported in several works previously [27, 30–32], at $T = 3100K$, below which their temperature dependence becomes Arrhenius. Relaxation times above this cross over temperature are well described by a power law form $\tau_\alpha \sim (T - T_c)^{-\gamma}$, as previously discussed [30, 34–36], with $T_c = 3100K$, and $\gamma = 1.5$. The value of γ is lower than reported in previous mode coupling analyses, which we do not attempt here. Instead, we simply note this as evidence for a fragile to strong crossover. In the case of KA BMLJ, previous analyses have estimated the mode coupling crossover temperature to be $T_c \sim 0.435$, and a fit to our data supports this identification. A γ value of 2.26 best describes our data, which is similar to values reported from mode coupling analyses previously [37–39].

Thus, in both cases, we conclude that the threshold

degree of annealing corresponds to a crossover temperature in the dynamics in the corresponding liquids. Although such an identification is merely an observation at present, it is made plausible and meaningful by numerous earlier studies, with associate the dynamical crossovers with a transition from diffusive to activated dynamics, and correspondingly, a change in the nature of the energy landscape sampled [32, 40–44]. Our results suggest that it may be fruitful to seek the common causes of the transition to brittle behavior of athermal glasses and changes in the character of dynamics in the corresponding liquids[45].

Summary

In summary, we have analysed the nature of yielding under cyclic shear deformation of two model glasses, the BKS silica glass, and the atomic model KA BMLJ, and found that for sufficiently well annealed glasses, yielding is strongly discontinuous, with the magnitude of discontinuity growing with the degree of annealing. Cyclic shear further offers a way for precisely identifying the threshold annealing/disorder through the qualitatively distinct responses above and below the annealing threshold. We show that for one of the models studied (KA BMLJ), uniform shear deformation reveals a change from ductile to brittle crossover that is consistent both with earlier analysis [20] and with the results of cyclic shear deformation. Finally, we find that the annealing threshold corresponds to well known dynamical crossover temperatures in the two systems we study, an observation that merits further analysis to understand their possible common origins. Whether the present results enable analysis of yielding at finite temperatures and strain rates, at least for well annealed glasses, along lines explored for crystals [46, 47] is another interesting question to pursue.

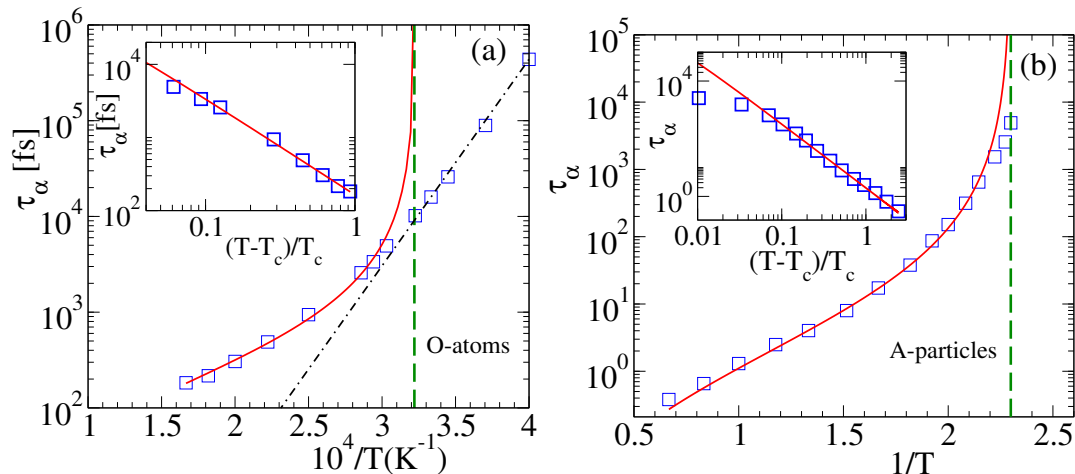


FIG. 4. **Dynamical crossover:** Plots of τ_α extracted from $F_S(k, t)$, shown as a function of the inverse temperature on a semi-logarithmic scale, for (a) silica and (b) BMLJ. The red solid lines through the data points are fits of the form $\tau_\alpha = \tau_0(T - T_c)^{-\gamma}$. For silica, the value of T_c and γ are 3100K (shown by the vertical dashed line) and 1.5 for the O-atom, and the dotted dashed line represents the Arrhenius temperature dependence low the temperature regime. For BMLJ, T_c and γ are found to be 0.435 and 2.26, respectively, for the A-particle.

APPENDIX

1. Models

The BKS potential [26] of silica we study, with modifications[27] to avoid unwanted divergences and treat long range forces properly, is given by

$$U(r_{ij}) = \frac{1}{4\pi\epsilon_0} \frac{q_i q_j}{r_{ij}} + \begin{cases} A_{ij} \exp(-B_{ij} r_{ij}) - C_{ij} r_{ij}^{-6} + \phi(r_{ij}) & r_{ij} \leq r_s \\ \sum_{k=3}^5 D_{ij}^k (r_{ij} - R_c)^k & r_s < r_{ij} < r_c \\ 0 & r_{ij} \geq r_c \end{cases} \quad (1)$$

where, the short-range term $\phi(r_{ij}) = 4\epsilon_{ij} \left[\left(\frac{\sigma_{ij}}{r_{ij}} \right)^{30} - \left(\frac{\sigma_{ij}}{r_{ij}} \right)^6 \right]$ is added for $r < r_s$ to prevent a negative divergence. The Coulomb term is evaluated by the Ewald summation technique with Ewald parameter $\alpha = 2.5 \text{ \AA}^{-1}$. The momentum space summation is carried out to a radius of six reciprocal lattice cell widths. The real part of the potential is truncated at $r_s = 7.7747 \text{ \AA}$. In the $r_s < r < r_c$ regime with $r_c = 10 \text{ \AA}$, a fifth order polynomial is added to make the potential go to zero smoothly. The coefficients of $\phi(r_{ij})$ are chosen such that the modified potential has no inflection at small r . The values of all the co-efficient can be found in Ref. [27]. An integration time step of 1fs is used.

The Kob-Andersen binary (80:20) mixture of Lennard Jones particles we study, with the interaction potential truncated at a cutoff distance of $r_{c\alpha\beta} = 2.5\sigma_{\alpha\beta}$ such that both the potential and the force smoothly go to zero, is

given by

$$V_{\alpha\beta}(r) = 4\epsilon_{\alpha\beta} \left[\left(\frac{\sigma_{\alpha\beta}}{r} \right)^{12} - \left(\frac{\sigma_{\alpha\beta}}{r} \right)^6 \right] + 4\epsilon_{\alpha\beta} \left[c_{0\alpha\beta} + c_{2\alpha\beta} \left(\frac{r}{\sigma_{\alpha\beta}} \right)^2 \right], r_{\alpha\beta} < r_{c\alpha\beta} \quad (2)$$

where $\alpha, \beta \in \{A, B\}$ and the parameters $\epsilon_{AB}/\epsilon_{AA} = 1.5$, $\epsilon_{BB}/\epsilon_{AA} = 0.5$, $\sigma_{AB}/\sigma_{AA} = 0.80$, $\sigma_{BB}/\sigma_{AA} = 0.88$. Energy and length are in the units of ϵ_{AA} and σ_{AA} respectively, and likewise, reduced units are used for other quantities. An integration time step of 0.005 is used.

2. Initial glass preparation

For both the models we performed constant volume, temperature (NVT) molecular dynamics simulations using the Nose-Hoover thermostat. The systems are equilibrated for $20\tau_\alpha$ for low temperatures, and for $10^3\tau_\alpha$, for the high temperature for silica, and more than $100\tau_\alpha$ for the KA BMLJ, τ_α being the structural relaxation time (see Fig. A9, *Appendix*).

For the KA BMLJ system, we generate inherent structures at energies lower than -7.00 through the finite temperature, shear rate annealing protocol explored in [33], with shear rate $\dot{\gamma} = 10^{-5}$, strain amplitude $\gamma_{max} = 0.035$ and simulation temperature $T = 0.3$. Further details of this procedure may be found in [33].

Independent configurations (between 5 and 12 for silica, and 6 for KA BMLJ) sampled from the equilibrium trajectory are subjected to energy minimization to obtain sets of inherent structures (IS) to be used for cyclic shear. Between 24 and 200 for $E_{IS} \leq -7.00$ and 12 for $E_{IS} > -7.00$ are used for uniform shear simulations. En-

ergy minimization is always (including AQS) performed

using the conjugate-gradient algorithm.

-
- [1] C. A. Schuh, T. C. Hufnagel, and U. Ramamurty, *Acta Materialia* **55**, 4067 (2007).
- [2] M. L. Falk and J. Langer, *Annual Review of Condensed Matter Physics* **2**, 353 (2011).
- [3] D. Bonn, M. M. Denn, L. Berthier, T. Divoux, and S. Manneville, *Reviews of Modern Physics* **89**, 035005 (2017).
- [4] A. Nicolas, E. E. Ferrero, K. Martens, and J.-L. Barrat, *Reviews of Modern Physics* **90**, 045006 (2018).
- [5] A. Wisitsorarak and P. G. Wolynes, *Proceedings of the National Academy of Sciences* **109**, 16068 (2012).
- [6] A. Wisitsorarak and P. G. Wolynes, *Proceedings of the National Academy of Sciences* **114**, 1287 (2017).
- [7] J. Lin, E. Lerner, A. Rosso, and M. Wyart, *Proceedings of the National Academy of Sciences* **111**, 14382 (2014).
- [8] D. Fiocco, G. Foffi, and S. Sastry, *Phys. Rev. E* **88**, 020301 (2013).
- [9] I. Regev, J. Weber, C. Reichhardt, K. A. Dahmen, and T. Lookman, *Nature Communications* **6**, 8805 (2015).
- [10] C. Rainone, P. Urbani, H. Yoshino, and F. Zamponi, *Physical review letters* **114**, 015701 (2015).
- [11] P. Urbani and F. Zamponi, *Physical Review Letters* **118**, 38001 (2017).
- [12] Y. Jin, P. Urbani, F. Zamponi, and H. Yoshino, *Science Advances* **4** (2018).
- [13] P. K. Jaiswal, I. Procaccia, C. Rainone, and M. Singh, *Phys. Rev. Lett.* **116**, 085501 (2016).
- [14] G. Parisi, I. Procaccia, C. Rainone, and M. Singh, *Proceedings of the National Academy of Sciences* **114**, 5577 (2017).
- [15] I. Procaccia, C. Rainone, and M. Singh, *Physical Review E* **96**, 032907 (2017).
- [16] T. Kawasaki and L. Berthier, *Phys. Rev. E* **94**, 022615 (2016).
- [17] P. Leishangthem, A. D. S. Parmar, and S. Sastry, *Nature Communications* **8**, 14653 (2017).
- [18] N. V. Priezjev, *Phys. Rev. E* **87**, 052302 (2013).
- [19] N. V. Priezjev, *Computational Materials Science* **150**, 162 (2018).
- [20] M. Ozawa, L. Berthier, G. Biroli, A. Rosso, and G. Tarjus, *Proceedings of the National Academy of Sciences* **115**, 6656 (2018).
- [21] M. Popović, T. W. de Geus, and M. Wyart, *Physical Review E* **98**, 040901 (2018).
- [22] A. D. S. Parmar, S. Kumar, and S. Sastry, *Phys. Rev. X* **9**, 021018 (2019).
- [23] Y. Shi and M. L. Falk, *Physical Review Letters* **95**, 95502 (2005).
- [24] Y. Shi, M. B. Katz, H. Li, and M. L. Falk, *Physical review letters* **98**, 185505 (2007).
- [25] S. Sastry, P. G. Debenedetti, and F. H. Stillinger, *Nature* **393**, 554 (1998).
- [26] B. W. H. van Beest, G. J. Kramer, and R. A. van Santen, *Phys. Rev. Lett.* **64**, 1955 (1990).
- [27] I. Saika-Voivod, F. Sciortino, and P. H. Poole, *Phys. Rev. E* **69**, 041503 (2004).
- [28] I. Saika-Voivod, F. Sciortino, and P. H. Poole, *Phys. Rev. E* **63**, 011202 (2000).
- [29] R. Chen, E. Lascaris, and J. C. Palmer, *The Journal of Chemical Physics* **146**, 234503 (2017).
- [30] J. Horbach and W. Kob, *Phys. Rev. B* **60**, 3169 (1999).
- [31] I. Saika-Voivod, P. H. Poole, and F. Sciortino, *Nature* **412**, 514 (2001).
- [32] A. Saksangwijit, J. Reinisch, and A. Heuer, *Phys. Rev. Lett.* **93**, 235701 (2004).
- [33] P. Das, A. D. Parmar, and S. Sastry, arXiv preprint arXiv:1805.12476 (2018).
- [34] J. Horbach and W. Kob, *Phys. Rev. E* **64**, 041503 (2001).
- [35] T. Voigtmann and J. Horbach, *Journal of Physics: Condensed Matter* **20**, 244117 (2008).
- [36] J. Horbach, *Journal of Physics: Condensed Matter* **20**, 244118 (2008).
- [37] W. Kob and H. C. Andersen, *Phys. Rev. Lett.* **73**, 1376 (1994).
- [38] W. Kob and H. C. Andersen, *Phys. Rev. E* **51**, 4626 (1995).
- [39] E. Flenner and G. Szamel, *Phys. Rev. E* **72**, 031508 (2005).
- [40] T. B. Schrader, S. Sastry, J. C. Dyre, and S. C. Glotzer, *The Journal of Chemical Physics* **112**, 9834 (2000).
- [41] K. Broderix, K. K. Bhattacharya, A. Cavagna, A. Zippelius, and I. Giardina, *Phys. Rev. Lett.* **85**, 5360 (2000).
- [42] L. Angelani, R. Di Leonardo, G. Ruocco, A. Scala, and F. Sciortino, *Phys. Rev. Lett.* **85**, 5356 (2000).
- [43] L. Angelani, R. Di Leonardo, G. Ruocco, A. Scala, and F. Sciortino, *The Journal of Chemical Physics* **116**, 10297 (2002), <https://doi.org/10.1063/1.1475764>.
- [44] E. La Nave, H. E. Stanley, and F. Sciortino, *Phys. Rev. Lett.* **88**, 035501 (2002).
- [45] W.-T. Yeh, M. Ozawa, K. Miyazaki, T. Kawasaki, and L. Berthier, (Submitted) (2019).
- [46] F. Sausset, G. Biroli, and J. Kurchan, *Journal of Statistical Physics* **140**, 718 (2010).
- [47] P. Nath, S. Ganguly, J. Horbach, P. Sollich, . S. Karmakar, and S. Sengupta, *Proceedings of the National Academy of Sciences* **115**, E4322 (2018).

APPENDIX

1. Inherent structure energy evolution with temperature

Here we show the behaviour of inherent structure energy E_{IS} for a wide range of temperatures for Silica and BMLJ, in Fig. A1 (a) and (b). For sufficiently high temperature T , the values of E_{IS} are show a plateau. For silica, E_{IS} data shows deviations from $1/T$ behaviour at low T as shown in the inset, discussed as an indication of the fragile-to-strong crossover in Ref. [31].

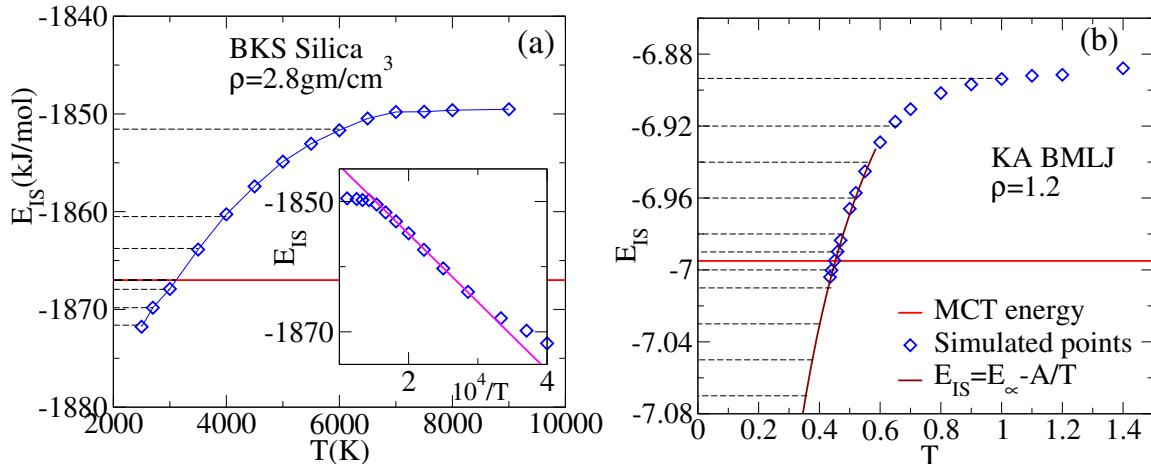


FIG. A1. Plot of inherent structure energy against temperature T for (a) silica and (b) BMLJ. For silica, each data point is sampled over 400 minimized configurations. For KA BMLJ the extrapolated curve is obtained by fitting equilibrium molecular dynamics simulation data to the equation: $E_{\infty} - A/T$ below the temperature $T = 0.7$ to obtain a mapping between the IS energy and temperature in the low temperature regime. Dashed horizontal lines represent the energy levels from which the IS-configurations are sampled to perform cyclic and uniform shear deformation. Horizontal red solid lines are indicating the threshold energy levels in the two models.

2. Energy as a function of accumulated strain for BKS Silica

The energy of the stroboscopic ($\gamma = 0$) configurations are shown in Fig. A2, as a function of the accumulated strain. Data are presented for both $T = 2500\text{K}$ and $T = 6000\text{K}$. As the yielding amplitude $\gamma_{max} = \gamma_y = 0.23$ is approached, the number of cycles to attain the steady state increases strongly. For both the temperatures, when $\gamma_{max} > \gamma_y = 0.23$, the same final energies are reached irrespective of initial values, which is not true for $\gamma_{max} < \gamma_y = 0.23$.

3. Stress-strain behavior over a cycle for BKS Silica

The stress-strain curves over a full-cycle for different strain amplitudes are shown in Fig. A3 for two different temperatures. The average stress values are calculated in the steady state.

4. Potential energy as a function of strain over multiple cycles for BKS silica

In Fig. A4, we show the evolution of the energy for two temperatures for a strain amplitude $\gamma_{max} = 0.20$ below yielding. For the low temperature case ($T = 2500\text{K}$) the system explores almost the same energy path for all cycles. For high temperature ($T = 6000\text{K}$), starting from a high energy state, the system anneals to a lower energy value around which it eventually remains oscillating.

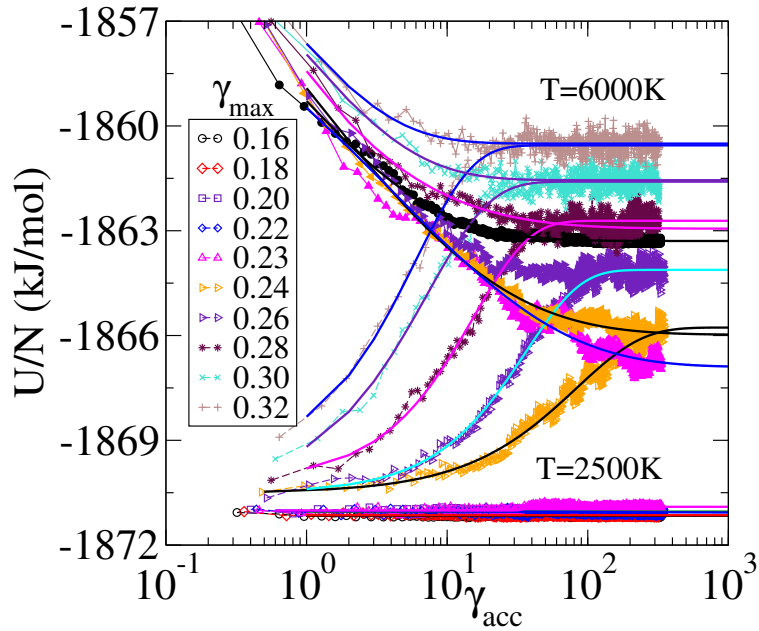


FIG. A2. Potential energy per particle U/N for zero-strain configurations, for $T = 2500\text{K}$ (lower set of curves, open symbols) and $T = 6000\text{K}$ (upper set of curves, filled symbols) for several strain amplitudes γ_{max} . Smooth solid lines through each data set are fits to a stretched exponential form from which the steady state energy values reported in Fig. 1 in the main text are obtained.

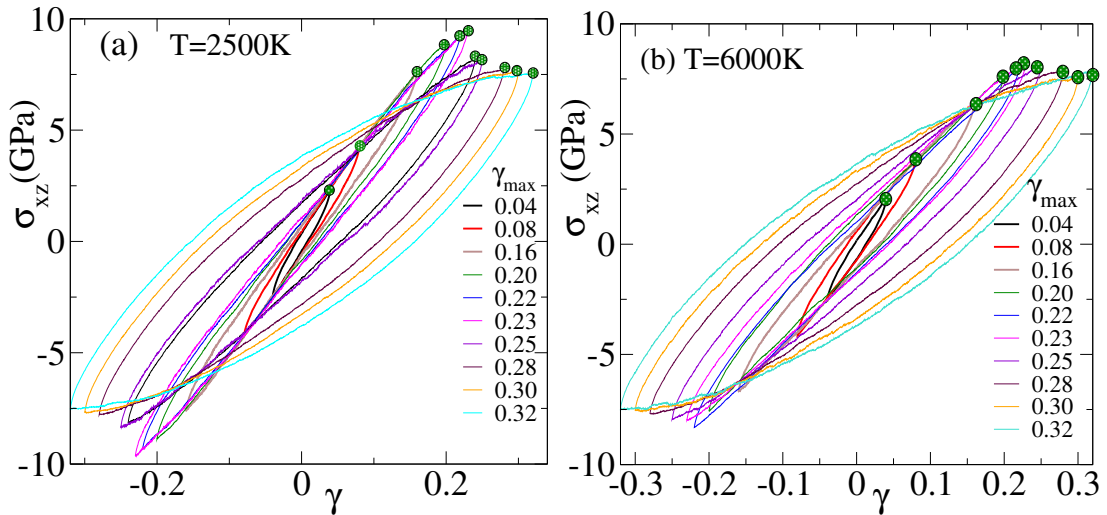


FIG. A3. **Stress strain behaviour of Silica under cyclic shear:** Plot of averaged stress against γ over a full cycle of deformation for different values of γ_{max} for (a) $T = 2500\text{K}$ and (b) $T = 6000\text{K}$. The curves are averaged over 10 samples and several cycles (≈ 30) for each sample in the steady state. Green dots represent the value of the maximum stress, at the strain amplitude, which are reported in Fig. 1 of the main text.

5. Energy as a function of accumulated strain for the Kob-Andersen BMLJ

In Fig. A5, we show the potential energy per particle U/N for stroboscopic configurations, as a function of the accumulated strain γ_{acc} for two differently annealed BMLJ systems with $E_{IS} = -7.07$ and -6.89 . The steady state value of U/N is obtained by fitting the data to a stretched exponential form, which are shown in Fig. 2 of the main text. For the well annealed case, below yielding amplitude, the energy of the system remains essentially constant. Above the γ_y , the energy increases with the number of shear cycles and reaches a steady state at longer times. For the poorly annealed glass, the energy always decreases with shear deformation cycles until it reaches a steady state.

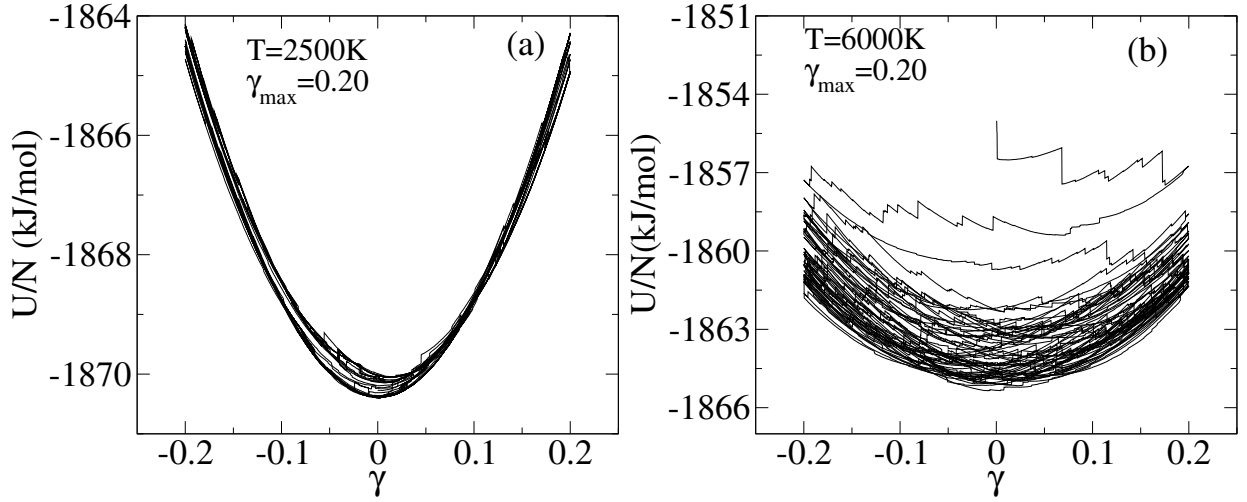


FIG. A4. **Potential energy vs. strain over multiple cycles for silica:** Plot of the potential energy over the cycles from the beginning of the simulations for (a) $T = 2500$ and (b) $T = 6000K$, at $\gamma_{max} = 0.20$.

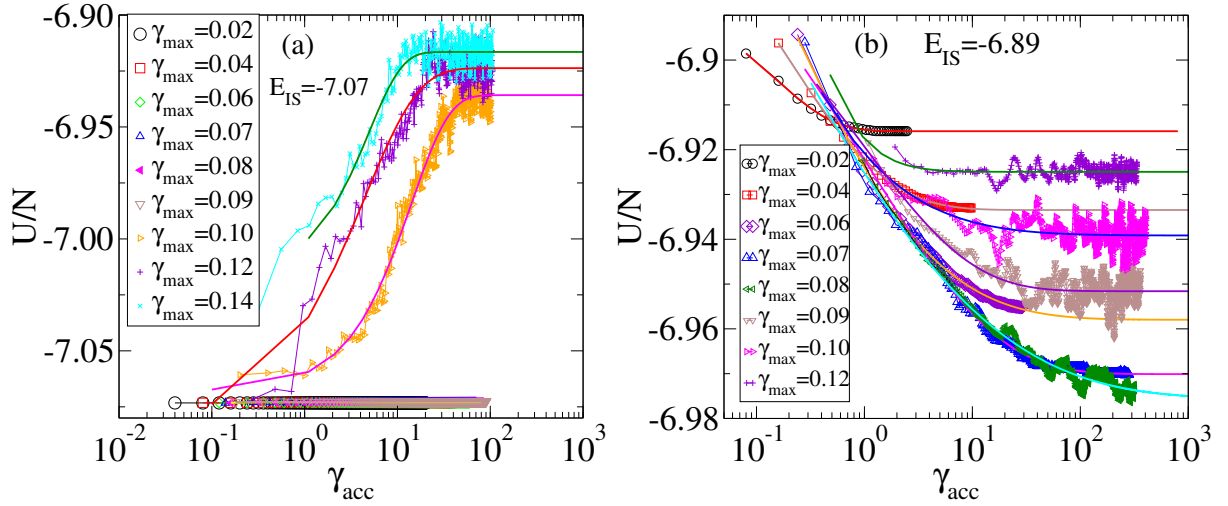


FIG. A5. **Approach to steady state for KA BMLJ:** Potential energy per particle U/N for zero-strain configurations plotted against accumulated strain γ_{acc} , (a) for $E_{IS} = -7.07$ and (b) for $E_{IS} = -6.89$. The data are averaged over 6 samples for the system size $N = 4000$. Solid lines through each data set are fits to a stretched exponential form.

6. Stress-strain behavior over a cycle for Kob-Anderson BMLJ

The averaged stress-strain curves in the steady state for a full-cycle of deformation for different strain amplitudes are shown in Fig. A6 for two different energies.

7. Potential energy as a function of strain over multiple cycles for the Kob-Andersen BMLJ

In Fig. A7, we show the potential energy of the KA BMLJ system for initial energies for strain amplitude $\gamma_{max} = 0.07$, below yielding. For the well annealed case ($E_{IS} = -7.07$), from the beginning of the strain cycles, the curves traverse essentially the same energies, while for the poorly annealed case $E_{IS} = -6.89$, starting from a high energy state, the system anneals to a lower energy value till it reaches the steady state.

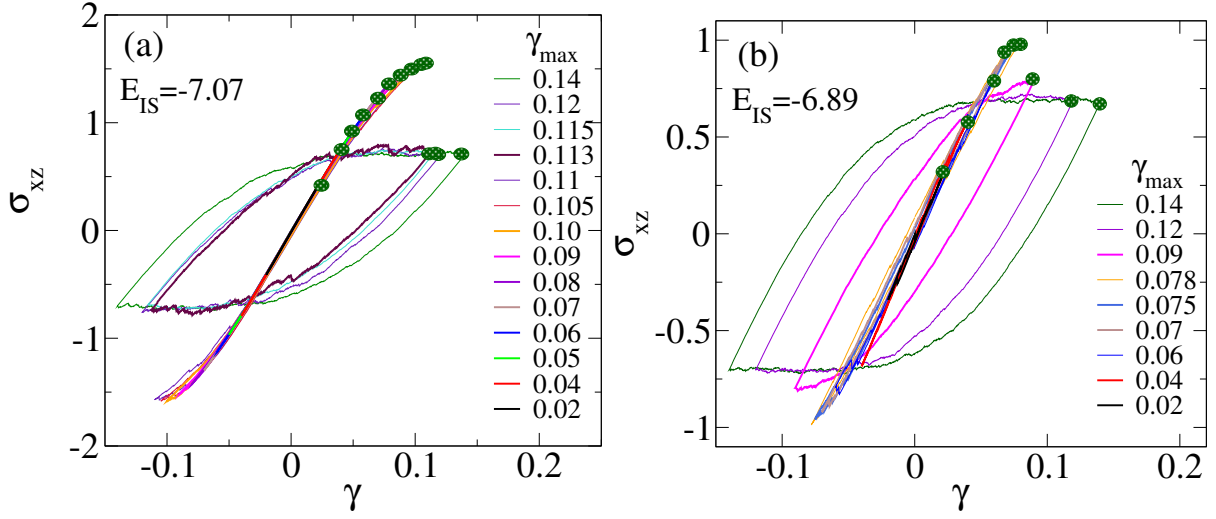


FIG. A6. **Stress strain behavior of BMLJ under cyclic shear:** Plot of stress as a function of γ over a full cycle of deformation for different strain amplitudes γ_{max} , averaged over several cycles in the steady state for (a) $E_{IS} = -7.07$ and (b) $E_{IS} = -6.89$. Green dots represent the maximum of stress reached by the system at the strain amplitude $\gamma = \gamma_{max}$.

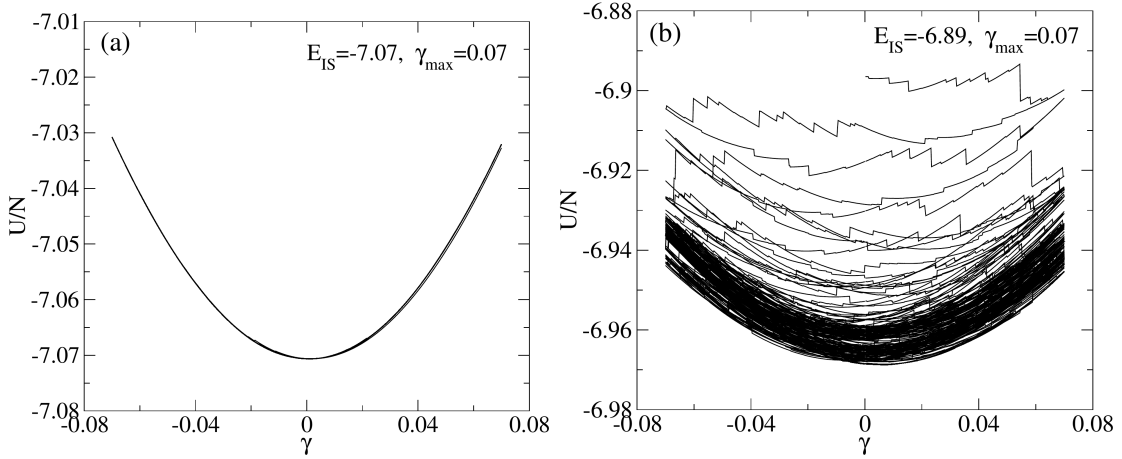


FIG. A7. **Evolution of potential energy:** Starting from the initial states, the potential energy is shown as they approach the steady state, for different inherent structure energies (a) $E_{IS} = -7.07$ and (b) $E_{IS} = -6.89$, for a strain amplitude below yielding, $\gamma_{max} = 0.07$. Note that for the deeply annealed glass ($E_{IS} = -7.07$) all the cyclic curves lie on top of each other indicating that very little annealing takes place. For the poorly annealed glass ($E_{IS} = -6.89$), the system anneals, lowering the energy till a steady state is reached.

8. Uniform shear deformation of KA BMLJ

We have studied the deformation of the KA BMLJ system under uniform shear. For such a study we consider a range of system sizes from $N = 2000$ to 64000 . We employ the AQS protocol with strain step $d\gamma = 0.0002$ and the strain varied from 0 to 0.3. For $N = 2000$, we considered 200 samples, for 4000 and $N = 8000$, 100 samples and for 32000 and 64000 we have considered 30 – 50 samples.

In addition to data presented in the main text, here we show the stress-strain curves for single samples for various cases. The evolution of the shear stress under uniform shear deformation is shown for different energies E_{IS} for a single sample of size $N = 64000$ in Fig. A8 (a). These curves reveal the emergence of large single stress drops as the degree of annealing increases. The stress response is shown in Fig. A8 (b) for different system sizes for a single sample of $E_{IS} (= -7.05)$ for each size. These results illustrate the manner in which the stress drops become focused in larger single drops at smaller strain values with an increase in system size.

We compute the connected susceptibility, defined as $\chi_{con} = -d\langle\sigma\rangle/d\gamma$, considering the stress averaged over 25 (40 for lowest system size) samples, computing mid-point numerical derivatives. The disconnected susceptibility, $\chi_{dis} = N[\langle\sigma^2\rangle - \langle\sigma\rangle^2]$ is obtained over the same sample set. We consider stress values within a window of $\Delta\gamma = 0.001$ for each sample, and obtain the mean and variance over this data set at each average strain value. Fig. A8 (c) and (d) show χ_{dis} as a function of E_{IS} for $N = 64000$ and for $E_{IS} = -7.05$ for different sizes respectively. The peak values in Fig. A8 (d) are shown in the inset as a function of system size. Fig. A8 (e) shows χ_{con} for $E_{IS} = -7.05$ for different sizes and the peak values are shown in the inset as a function of system size. Finally, in Fig. A8 (f), we show the dependence on E_{IS} , for various system sizes, of the maximum stress drop observed in a range of strain values from 0 to 0.15, straddling the yield strain. We subtract the value of the stress drop at $E_{IS} = -6.89$, which corresponds simply to the drops in the post-yield flow regime. The maximum stress drop shows little system size dependence above the threshold value of $E_{IS} = -6.99$ but grows strongly with system size below, indicating the increasingly strong discontinuous yielding at lower E_{IS} or higher annealing.

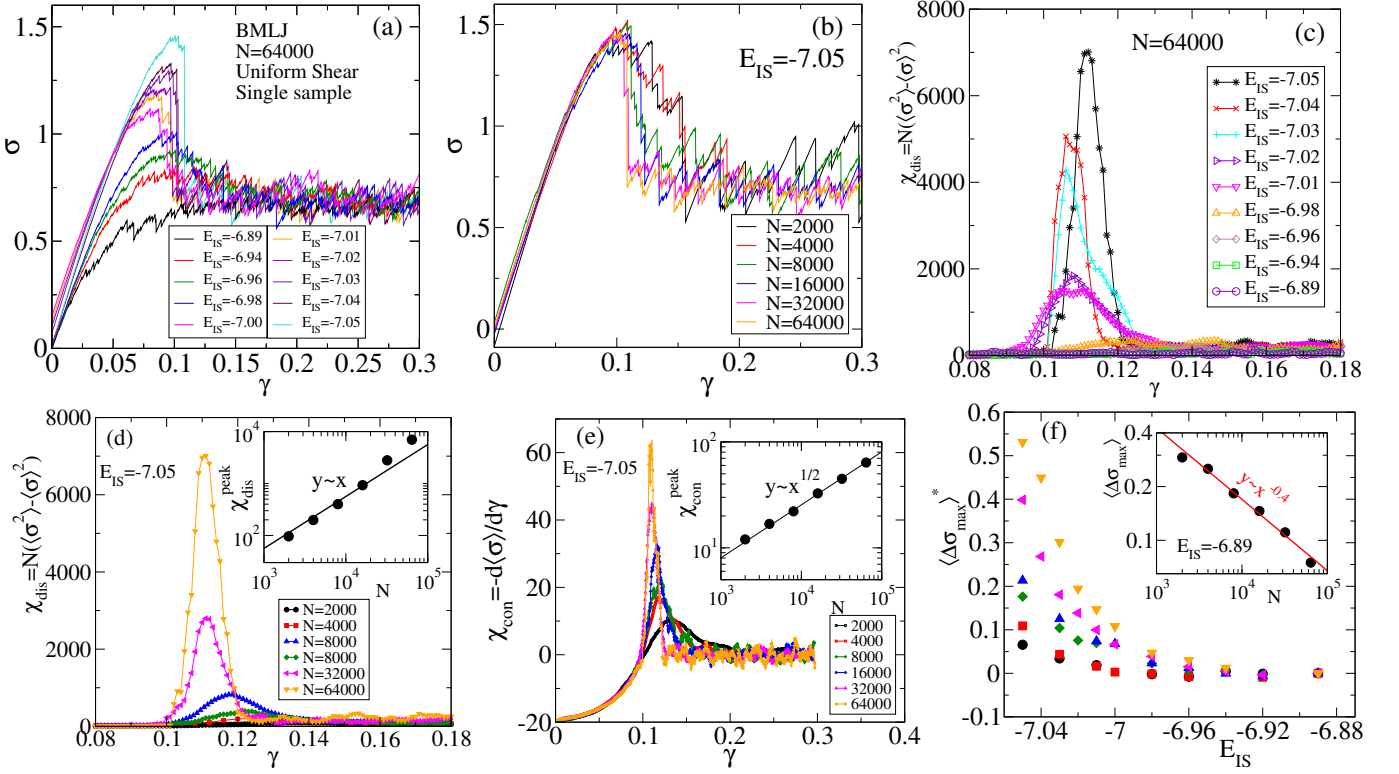


FIG. A8. **Uniform shear of KA BMLJ:** (a) Stress-strain curves for different E_{IS} for a single sample, for the system of size $N = 64000$. (b) Stress-strain curves for a single sample for $E_{IS} = -7.05$ for different system sizes. (c) Fluctuations in the stress (disconnected susceptibility) against γ for different E_{IS} , $N = 64000$. (d) Disconnected and (e) connected susceptibility for different system sizes. Corresponding insets show the scaling of peak of susceptibility against N showing $\chi_{dis}^{peak} \sim N$ and $\chi_{con}^{peak} \sim N^{1/2}$ scaling, respectively. (f) Plot of $\langle\Delta\sigma_{max}\rangle^* \equiv \langle\Delta\sigma_{max}\rangle - \langle\Delta\sigma_{max}\rangle_{E_{IS}=-6.89}$, $\langle\Delta\sigma_{max}\rangle$ being the average maximum drop, against initial inherent structure for different system sizes. Inset: Plot of average maximum stress drop $\langle\Delta\sigma_{max}\rangle$ with system size N for $E_{IS} = -6.89$.

9. Intermediate scattering function

In order to calculate the relaxation time of dynamics of liquid we have calculated the self part of the intermediate scattering function $F_s(k, t)$. For A-type of particles (equivalently for Si and O atoms of silica) the $F_s(k, t)$ is defined as,

$$F_s(k, t) = \frac{1}{N_A} \sum_{j=1}^{N_A} \langle \exp[i\mathbf{k} \cdot (\mathbf{r}_j(t) - \mathbf{r}_j(0))] \rangle$$

where k is the wave vector (with values used given the figure caption), r_i is the particle coordinate and N_A is the number of A-type atoms in the system. The calculated values of $F_s(k, t)$ are shown in Fig. A9 for Oxygen and Silicon atoms for silica and for the A-type particles for BMLJ for a wide range of temperatures. The relaxation times τ_α obtained from the stretched exponential fits are shown in Fig. 4 of the main text.

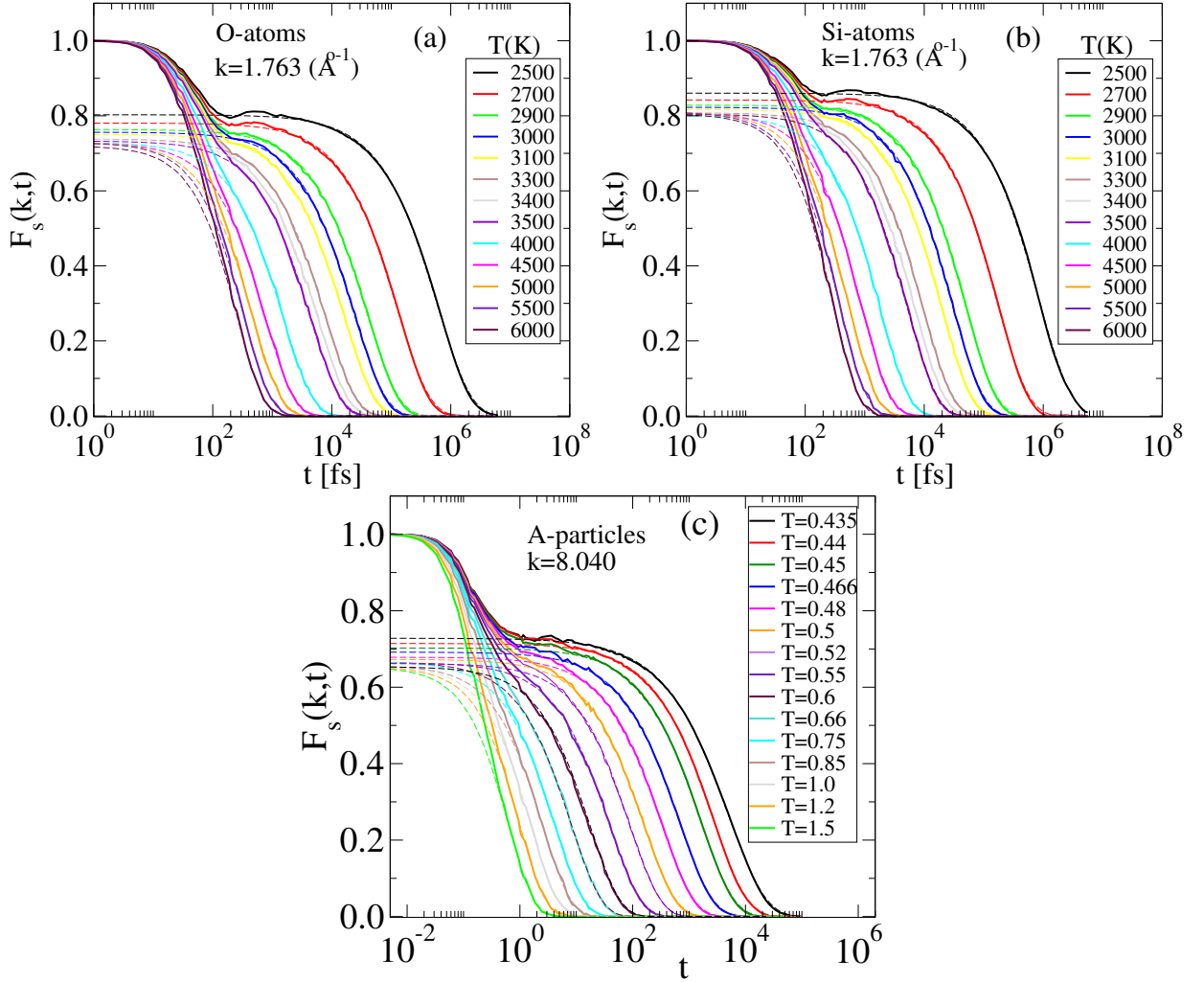


FIG. A9. **Self intermediate scattering function of liquid silica and liquid BMLJ:** Plot of the self part of the intermediate scattering function $F_s(k, T)$ for (a) Oxygen and (b) Silicon atoms at different temperatures for a system of size $N = 1728$ for $k = 1.76 \text{ \AA}^{-1}$. Dashed lines are fits to the form $f(t) = f_c[\exp(-t/\tau_\alpha)^\beta]$. (c) Plot of $F_s(k, T)$ of A-type of particles for the KA BMLJ model for different temperatures. System size considered here is $N = 4000$ and $k = 8.04$.